Journal of
Manufacturing and Materials Processing

MDPI

Article

Performance Characterization of Laser Powder Bed Fusion Fabricated Inconel 718 Treated with Experimental Hot Isostatic Processing Cycles

Jaime Varela [1,2], Jorge Merino [2,3], Christina Pickett [2,3], Ahmad Abu-Issa [1,2], Edel Arrieta [1,2], Lawrence E. Murr [2,3], Ryan B. Wicker [1,2], Magnus Ahlfors [4], Donald Godfrey [5] and Francisco Medina [1,2,*]

1 Department of Mechanical Engineering, The University of Texas at El Paso, El Paso, TX 79938, USA; jvarela11@miners.utep.edu (J.V.); aoabuissa@miners.utep.edu (A.A.-I.); egarrieta@utep.edu (E.A.); rwicker@utep.edu (R.B.W.)
2 W.M. Keck Center for 3D Innovation, University of Texas at El Paso, El Paso, TX 79968, USA; jimerinogomez@miners.utep.edu (J.M.); cdpickett@miners.utep.edu (C.P.); lemurr@utep.edu (L.E.M.)
3 Department of Metallurgical, Materials and Biomedical Engineering, The University of Texas at El Paso, El Paso, TX 79968, USA
4 Quintus Technologies LLC, Lewis Center, OH 43035, USA; magnus.ahlfors@quintusteam.com
5 Honeywell Aerospace, Phoenix, AZ 85034, USA; donald.godfrey@honeywell.com
* Correspondence: frmedina@utep.edu

Received: 25 June 2020; Accepted: 17 July 2020; Published: 21 July 2020

Abstract: Inconel 718 alloy fabricated by selective laser melting (SLM) (or laser powder-bed fusion (LPBF)) has been post-process heat-treated by stress-relief anneal at 1065 °C; stress-relief anneal (1065 °C) + solution treatment (at 720 °C) + aging (at 620 °C); hot isostatic pressing (HIP) (at 1120–1200 °C); stress-relief anneal + HIP; and stress-relief anneal + HIP + solution treatment + aging. Microstructure analysis utilizing optical metallography revealed primarily equiaxed grain structures (having average diameters ranging from ~30 to 49 microns) containing annealing twins, and a high concentration of carbide precipitates in all HIP-related treatments in the grain boundaries and intragrain regions. However, no precipitates nucleated on the {111} coherent annealing twin boundaries because of their very low interfacial free energy in contrast to regular grain boundaries. The mechanical properties for the as-fabricated Inconel 718 exhibited a yield stress of 0.64 GPa, UTS of 0.98 GPa, and elongation of 26%. Following stress-relief anneal at 1065 °C, the yield stress dropped to 0.60 GPa, while the elongation increased to 43%. The associated grain structure was an irregular, somewhat elongated, recrystallized structure. This structure was preserved at a stress anneal at 1065 °C + solution treatment + aging, but grain boundary and intragrain precipitation resulted in a doubling of the yield stress to 1.3 GPa and a reduced elongation of 12.6%. The results of HIP-related post-process heat treatments involving temperatures above 1060 °C demonstrated that the yield stress and elongations could be varied from 1.07 to 1.17 GPa and 11.4% to 19%, respectively. Corresponding Rockwell C-scale hardness values also varied from 33 for the as-fabricated Inconel 718 to 53 for simple post-process HIP treatment at 1163 °C.

Keywords: additive manufacturing; inconel 718; HIP; heat Treatment; laser powder bed fusion; microstructures; mechanical properties

1. Introduction

Since its development at Pratt–Whitney in the early 1960s, Inconel 718 has been the most widely used Ni-base superalloy in the aircraft and aerospace industry, especially in high-temperature turbine

applications. It has also found extensive use in the broad array of energy industries [1–5]. Its utility is mainly derived from the ability to tailor a wide range of mechanical properties, which include homogenization and stress-relief anneals, solution treatment, and aging. Its nominal composition of 50–55 wt % Ni, 12–21 wt % Cr, and 4.75–5.5 wt % Nb accounts for a melting temperature of around 1430 °C and a density of ~8.2 g/cm^3, both of which can vary with specific compositions. Heat treatment strategies produce primarily fcc gamma-prime (Ni_3(Nb,Ti)) precipitate spheroids or cuboids at varying length scales (nano-to-micron), bct gamma-double prime (Ni_3Nb) disc-like precipitates coincident with {001} planes in the fcc Ni-Cr (gamma) matrix; and needle-like plates of delta phase (Ni_3Nb). Small additions of carbon in the composition can form a variety of carbides in the grain boundaries and the matrix, and a host of brittle Laves $(Ni,Fe,Cr)_2(Nb,Mo)$ phase precipitates, which are deleterious to mechanical properties, can also form [2–5]. Strengthening in commercial cast and wrought Inconel 718 alloy products occurs by solutionizing and aging treatments to adjust the gamma-prime/gamma-double prime volume fraction, which can produce Rockwell C-scale hardnesses (HRC) ranging from ~20 to 50, tensile strengths ranging from 1 to 1.4 GPa, UTS ranging from 1.2 to 1.5 GPa, and elongations ranging from ~12% to 25% [2–5].

With the recent development of additive manufacturing (AM) technologies, especially involving laser and electron beam powder-bed fusion fabrication, Inconel 718 alloy has received renewed attention because of its continuing prominence in the aerospace and energy industries, as well as the ability of AM to achieve complex and cost-effective component geometries often impossible to fabricate by conventional manufacturing [6–12]. The many recent selective laser melting (SLM) and electron beam melting (EBM) studies [6–12] have also included a wide range of post-process heat treatment strategies to continue to provide selective and optimized mechanical properties specifically suited to applications of these novel products. In addition, since precursor, pre-alloyed powders can contain inert gas bubbles as a consequence of the atomization process, and scanning errors can create poor powder sintering and melting, the resulting porosities in fabricated products can be a concern. Residual stresses are also often a concern in the SLM process in contrast to the EBM process. Consequently, hot isostatic processing (HIP) poses some advantages in post-process heat treatment. However, HIP presents its own issues as a consequence of the high temperatures involved, which can dissolve strengthening microstructures and create unwanted grain growth, generally degrading the mechanical properties.

In this study, new HIP strategies were investigated for SLM-processed Inconel 718 by incorporating high temperature and standard low-temperature solutionizing and aging treatments to examine heat treatment strategies for optimum mechanical properties. These are associated with carbide precipitation-strengthened, small (30–50 micron) grain structures that provide nominal tensile strengths above 1 GPa, and corresponding elongations greater than 11%.

2. Materials and Methods

2.1. Powder Feedstocks

Gas-atomized Inconel 718 powder was provided by Praxair (Danbury, CT, USA). The powder was analyzed for particle size and shape using a Retsch Camsizer X2 (Haan, Germany). The Camsizer is a Dynamic Image Analysis, which allows for the reliable measurement of particle shape and particle size distribution. Analysis revealed an average particle size of ~30 µm from a range of particle sizes of ~18 to 46 µm. Furthermore, the powder was examined through an SEM using a JEOL JSM-IT500 (Tokyo, Japan), as illustrated in Figure 1.

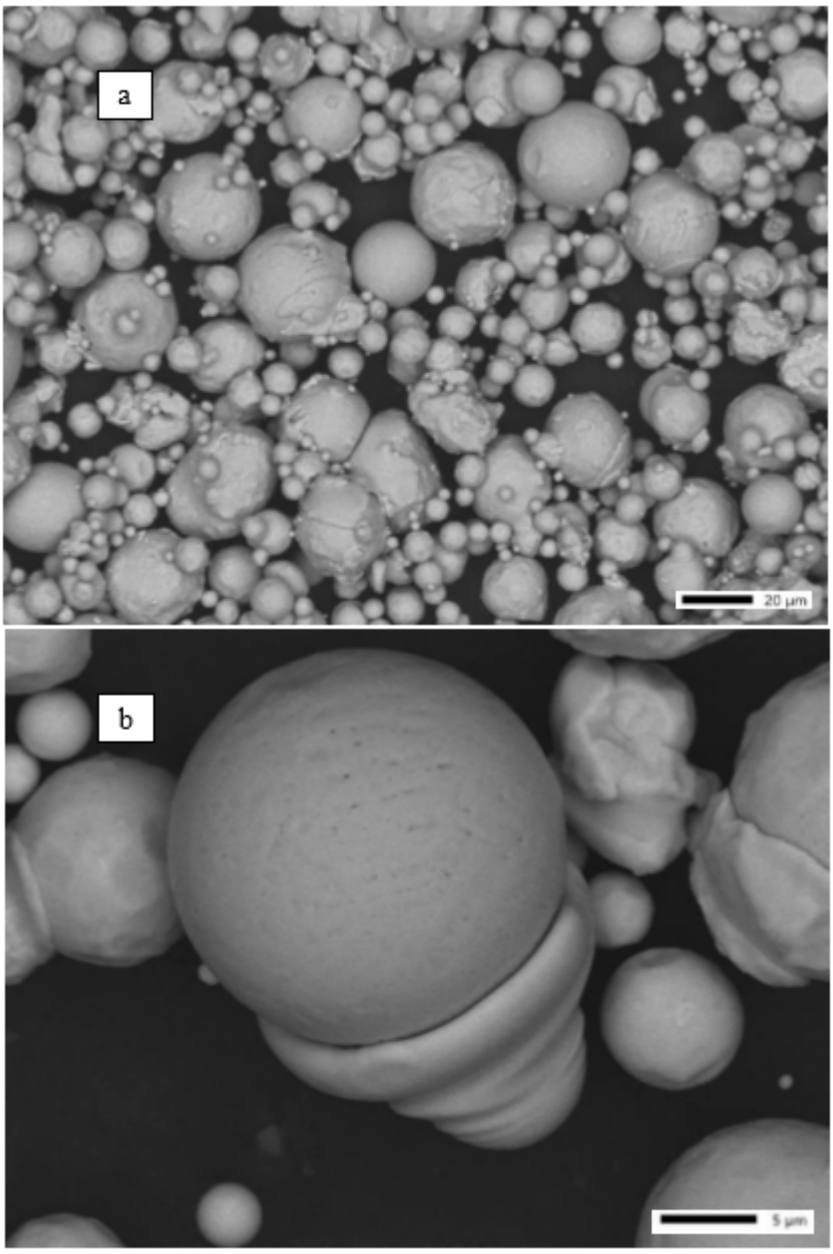

Figure 1. Prealloyed, atomized Inconel 718 powder SEM images. (**a**) Low magnification. (**b**) High magnification.

2.2. Laser Powder Bed Fusion Systems, Setup, and Fabrication

The EOS M290 (Krailling, Germany) is an industrial production LPBF system with a 250 × 250 × 325 mm build volume. It utilizes a 400 W Ytterbium fiber laser. A total of 105 vertical cylinders were fabricated by Honeywell Aerospace in this system. The fabricated cylinders had an average length of 10 cm.

2.3. Process Parameters

Inconel samples were fabricated on a preheated bedplate at 80 °C. The laser operated at 285 W at a speed of 960 mm/s. Laser scans were separated with a hatching distance of 0.11 mm. A striped width of 10 mm with a 0.12 mm overlap was utilized. The beam had a diameter of 100 µm. A 40 µm layer thickness was used.

2.4. Hot Isostatic Pressing Parameters for Post-Processing Heat Treatment

HIP is a process in which a part is inserted in a chamber with inert gas and subjected to high temperatures and high pressure. The temperatures typically range from 80 to 90% of the melting temperature and pressures higher than that of the yield strength of the part. This induces plastic deformation and diffusion bonding to eliminate interior micro defects. In this project, eleven variants were created, all with different combinations of HIP and heat treatment (HT), both in and out of HIP. Samples were subjected to stress-relief anneal (SR), HIP, Solution Annealing (SA) and Ageing (Age) (SAE AWS 5662 (2016)) in and out of HIP, and high temperature solutionizing as denoted in Table 1 below, in a QIH9 system with a Uniform Rapid Cooling furnace (Quintus Technologies LLC, Lewis Center, OH, USA).

Table 1. Hot Isostatic Pressing and Heat Treatment Parameters.

Variant	Process	Pressure (psi)	Temperature (°C)	Hold Time (min)	Cooling Rate (°C/min)
1	SR	None			
	HIP				
	SA				
	Age				
2	SR	none	1065	90	
	HIP	None			
	SA				
	Age				
3	SR	none	1065	90	
	HIP	none			
	SA	none	720	480	
	Age	none	620	480	
4.1	SR	none	1065	90	
	HIP	none	1120	240	
	SA	none	720	480	
	Age	none	620	480	
4.2	SR	none	1065	90	
	HIP *	15,000	1163	180	~150
	SA	none	720	480	
	Age	none	620	480	
5	SR *	12,000	1066	60	~150
	HIP *	15,000	1163	180	
	SA	none	720	480	
	Age	none	620	480	
6	SR	none	1065	90	
	HIP *	15,000	1163	180	~150
	SA *	12,000	1060	20	
	Age	none	620	480	

Table 1. *Cont.*

Variant	Process	Pressure (psi)	Temperature (°C)	Hold Time (min)	Cooling Rate (°C/min)
7	SR	none	1065	90	~1500
	HIP *	15,000	1163	180	
	SA *	14,200	1060	20	
	Age	none	620	480	
8	SR *	10,000	1066	60	~150
	HIP *	15,000 + 12,000	1163 + 1060	180 + 20	
	SA *	10,000	720	480	
	Age *	10,000	620	480	
9.1	SR	none	1065	90	~150
	HIP *	15,000	1105	180	
	SA *	15000	720	480	
	Age	none	620	480	
9.2	SR	none	1065	90	~150
	HIP *	15,000	1200	180	
	SA *	15,000	720	480	
	Age	none	620	480	

* Heat treatment done in hot isostatic processing (HIP) machine.

Table 1 involves a wide range of heat treatment schedules designed to examine the ability to select desirable residual mechanical properties, and the efficacy of HIP in heat treatment considering that HIP generally involves temperatures above that which induces rapid recrystallization (~1050 °C) [13,14]. While, as described briefly in the Introduction, Inconel 718 can be variously manipulated by heat treatment to produce a range of mechanical property (tensile) behavior (including yield stresses in excess of 1.2 GPa and corresponding elongations >10%) as a consequence of a wide range of induced precipitation [5–12], recrystallization can restrict these strategies. Consequently, and as shown in Table 1, HIP temperatures well above the rapid recrystallization temperature are expected to restrict more conventional heat treatment strategies, especially those involving solution annealing (SA) and aging (Age) treatments.

2.5. Microstructure Characterization

Samples from each variant were sectioned for metallographic analysis. Each tensile specimen was sectioned at the unstrained threaded sections, which had an approximate dimension of 10 mm for the diameter and 15 mm for the length. This was done to study the sections of the specimen that were not affected by the tensile test, thereby not disrupting the representation of the microstructure. The samples were sectioned such that it would reveal the *X*, *Y*, and *Z* planes. The metallographic samples were created using an ATM OPAL 460 (Haan, Germany) hot mounting press and black epoxy. All metallographic samples were ground and polished using an ATM SAPHIR 530 semi-automatic system. The samples began being ground with a resin-bonded diamond grinding disc with a grit of 120 at 300 rpm with 35 N of force until plane. They then moved onto a fine grinding pad using a 9 µm diamond suspension at 150 rpm with 35 N of force for 5 min. Samples were fine polished with a woven acetate cloth and a 1 µm diamond suspension at 150 rpm and 35 N of force for 5 min.

The microstructure was revealed using Kalling's No. 2 reagent, which consisted of 5 g of Copper Chloride, 100 mL of Hydrochloric Acid, and 100 mL of Ethanol. The etching was performed immediately after the last step of polishing in order to avoid oxidation. Every variant reacted at

different times of exposure ranging from 3 s to 60 s. Variant 1 was etched using a cotton swabbing method. Variants 2 to 9.2 were electro-etched at 5 V for varying times. Microstructure was studied on the inverted optical microscope Olympus™ GX53 (Olympus Inc., Tokyo, Japan).

2.6. Density Measurements

Volume measurements were performed on an AccuPyc II 1340 (Norcross, GA, USA) gas displacement pycnometer. Mass measurements were then performed on a Sartorius CP124S weight balance (Sartorius AG, Gotinga, Germany). The resulting average of the volume was divided by the mass, giving the density.

2.7. Tensile Testing

All post-processed and as-printed samples were machined and threaded according to ASTM E8. Monotonic uniaxial tensile strength tests were performed on all specimens. An MTS Landmark (Eden Prairie, MN, USA) servo-hydraulic system, with a force capacity of 100 kN, equipped with threaded grips, was used. The displacement (strain) rate was 0.15 mm/min. An MTS 30 mm axial clip extensometer was utilized for axial strain measurement. The results were averaged from 6 specimens for each variant.

2.8. Hardness Testing

Hardness measurements were obtained with a Struers Duramin-A300 (Ohio, OH, USA) on a Rockwell C scale. Measurements were performed at the top and bottom sections of the specimen in the X, Y, and Z cross-sections. A 5 s dwell time with a load of 100 gf was used for the indentations. Four evenly distributed indentations were performed on each surface of every specimen, separated by at least one millimeter.

2.9. Grain Size Measurements

Grain size measurements were obtained according to ASTM E 112 using the mean intercept method. Average grain size estimation was done by counting the number of grain boundaries intercepting one or more straight lines in order to attain at least 100 intercepts. Annealing twin boundaries were included as intercepting boundaries.

3. Results and Discussion

3.1. Microstructure Analysis and Discussion

Figure 2a,b show the as-built (Variant 1) microstructures to consist of the traditional (SLM) melt band structure (Figure 2a) and an inter-band cellular dendritic microstructure within small grain domains (~18 microns) (Figure 2b) similar to the microstructures described in previous studies of Inconel 718 [7,10]. There are no prominent columnar grain structures in Figure 2b as described in the work of Helmer et al. [15] and Keshavarskerwani et al. [16], and this is due to the selection of processing parameters, which as discussed in a recent review by DebRoy et al. [17], control the development of solidification maps, which determine the residual microstructures. These microstructures (in Figure 2b) are compared with the microstructure characteristic of the stress-relief anneal (Variant 2) at 1065 °C (Table 1), as shown in Figure 2c, where the melt bands have annealed out and the cellular dendritic structure has been recrystallized to form elongated and irregular, and even serrated grains having a nominal size of ~22 microns. It is notable that the stress-relief temperature is just above that which is characteristic of rapid recrystallization in Inconel 718 [13,14]. The Rockwell C-scale hardness (HRC) declined from 38 for the as-built Inconel 718 product (Figure 2b) to 33 for the stress-relief anneal product (Figure 2c).

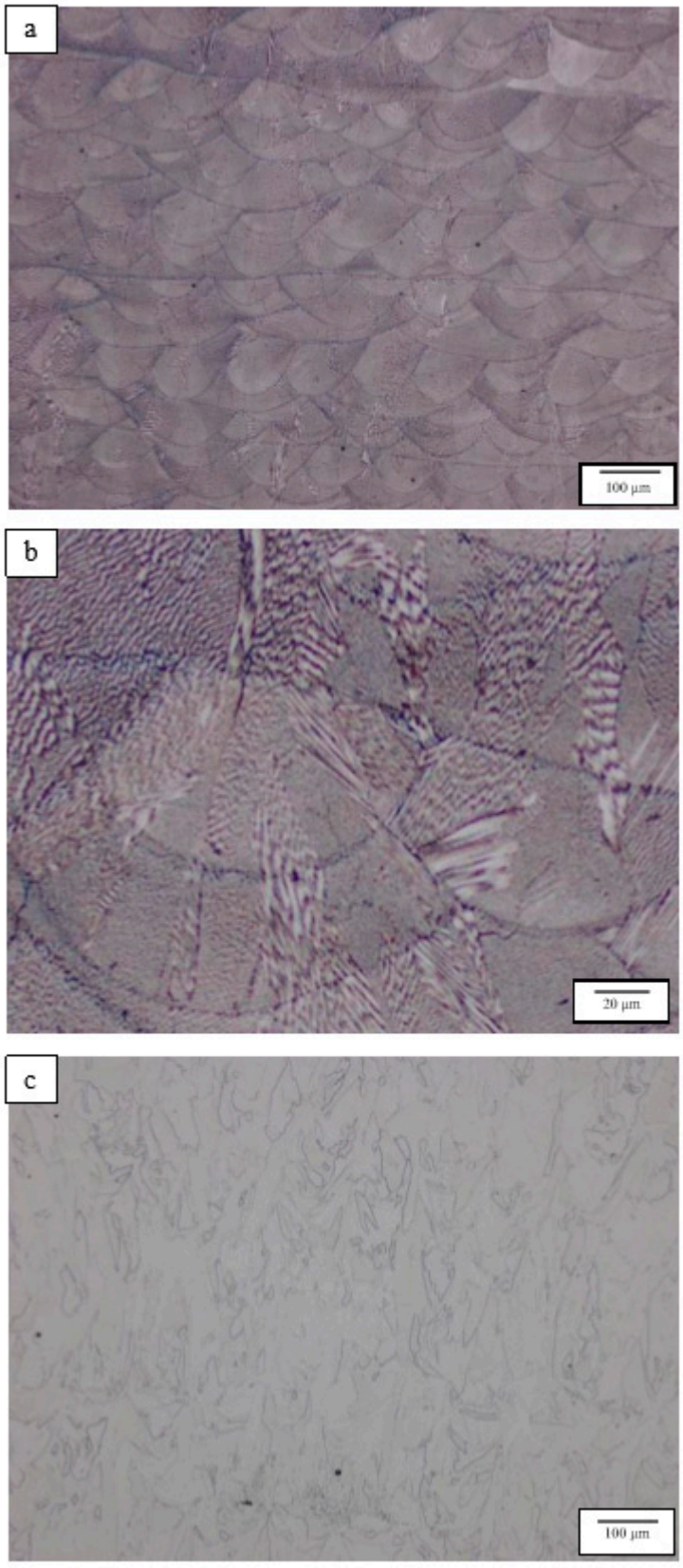

Figure 2. Optical metallography (OM) image of as-built (Variant 1) Inconel 718 alloy component (**a**). (**b**) shows a magnified image of (**a**). (**c**) As-built and stress-relief annealed 718 alloy (Variant 2) (Table 1).

Figure 3a,b, in contrast to Figure 2, compare the stress-relief anneal plus solutionizing and aging heat treatment (Table 1), with no HIP (Variant 3) (Figure 3a), with stress-relief anneal at 1065 °C and HIP at 1163 °C for 3 h (Variant 4.2 in Table 1). There is only slight grain growth in Figure 3a, in contrast to Figure 2c—from 22 microns to 24 microns—while Figure 3b shows complete recrystallization forming equiaxed grains (~39 microns) and containing profuse annealing twins [13,14], and precipitates in both the grain boundaries and the grain interiors. The corresponding HRC values for Figure 3a,b were ~54 and 53, respectively; an increase of ~42% from Figures 2c and 4a,b show these microstructures (for Figure 3a,b) at higher magnifications, whereas in Figure 4a there are prominent precipitates along the grain boundaries and with the grains, as well as numerous, faint parallel precipitate-like features within the grains. Clearly, these microstructures account for the prominent hardness increase. In contrast, Figure 4b shows prominent precipitates within the grain boundaries and the intra-grain regions as well, but these precipitates are notably different from those in Figure 4a, and are likely to be MC carbides, since all other precipitate phases (gamma prime, gamma double-prime, delta, and other carbides) have solvus temperatures below the 1163 °C HIP temperature the specimens in Figure 4b were subjected to (Table 1) [18–20].

It is also notable to observe in Figures 3b and 4b that while carbides appear in the grain boundaries, there are no carbides in the straight {111} fcc coincident annealing twin boundaries. This is especially prominent in Figure 4b at the large twin grain at the lower-left portion of the image, where precipitates are absent along the coherent (straight) boundaries, but occur at the steps at the end of the twin grain; the non-coherent twin boundary segments. This phenomenon has been observed and described for heat-treated 304 stainless steel by Trillo and Murr [21], as well as more recent EBM cladding of Inconel 690 on 316 stainless steel substrates aged at 685 °C for 50 h [22]. This occurs because coherent {111} annealing twin boundaries have very low interfacial free energies in contrast to the non-coherent boundary steps and the regular grain boundaries, thereby retarding carbide nucleation and precipitation [23]. Interestingly, Da Cruz Gallo, et al. [24] have also described similar interfacial energy preferences for delta phase precipitation in Hot-rolled Inconel 718 forgings.

Variants 5, 6, and 7, heat treated as shown in Table 1, exhibited microstructures essentially the same as Figures 3b and 4b, with grain sizes ranging from 32 to 35 microns, and corresponding hardness (HRC) values ranging from 49 to 52. Figure 5a,b illustrate these features for Variants 6 and 7, respectively. While Variant 8 represents a complex heat treatment cycle, as shown in Table 1, the solutionizing and aging were performed in the HIP regime, and the microstructures were unchanged from Figure 5. This is illustrated in Figure 6, which also compares Variant 8 with Variant 9.2 (Table 1) HIPed at 1200 °C. The higher temperature associated with Variant 9.2 (Figure 6b) is reflected in a grain size of ~49 microns in contrast to Figure 6a where the grain size was 33 microns.

It is apparent in comparing Figure 3b through Figure 6, that HIP treatments at temperatures of 1163 °C up to 1200 °C, well above the rapid recrystallization temperature of ~1050 °C for Inconel 718 [13,14], control the residual heat treatment microstructures (or grain sizes, which only vary from 33 to 49 microns) as well as the corresponding hardnesses, which only vary from 51 to 53 HRC. These hardness values are determined by the formation of carbides, which are stable up to ~1250 °C. Consequently, when HIP treatments are used, the HIP temperature becomes the controlling feature for determining the mechanical properties.

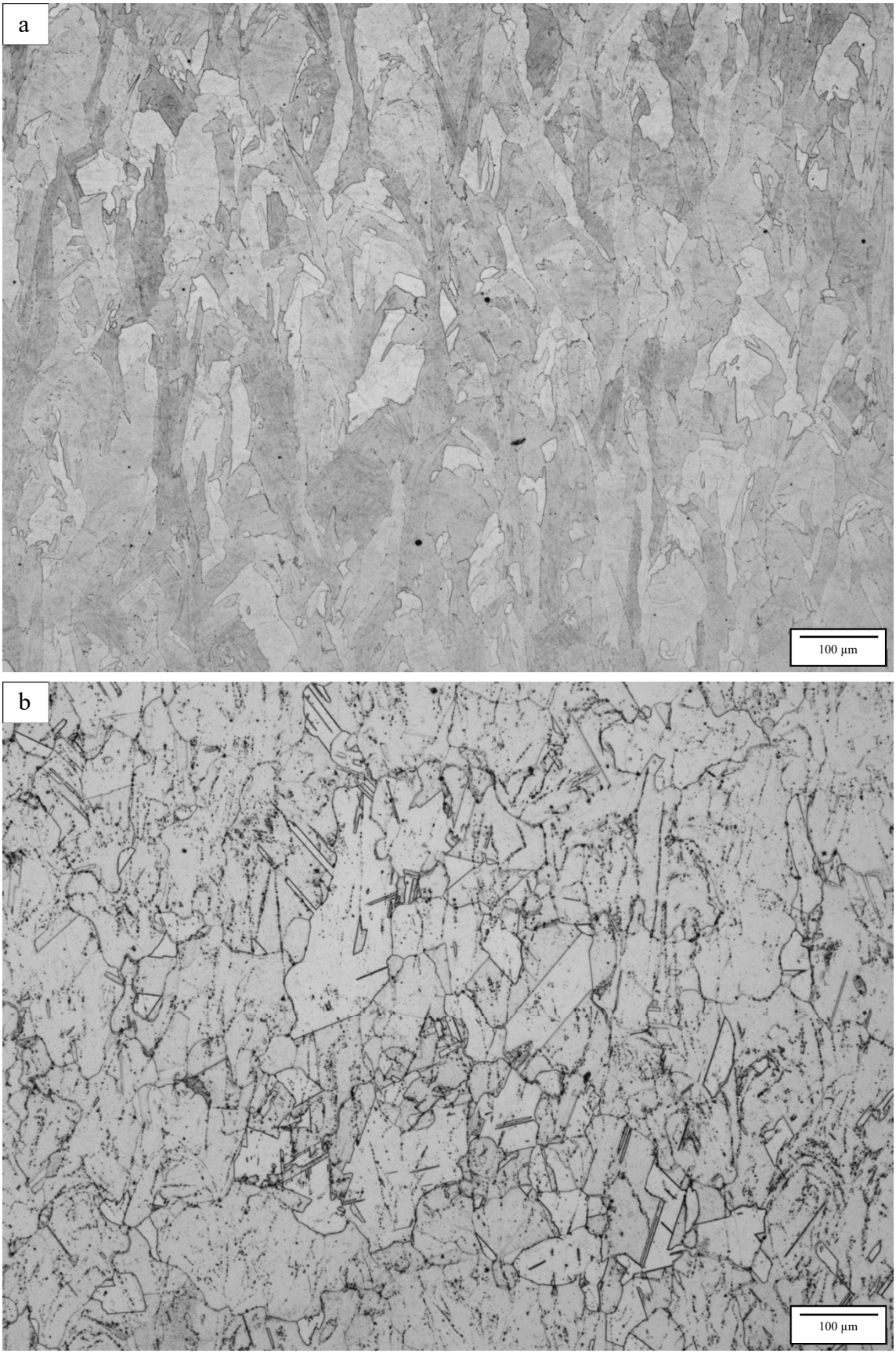

Figure 3. OM image of Variant 3 (**a**) and Variant 4.2 (Table 1) (**b**).

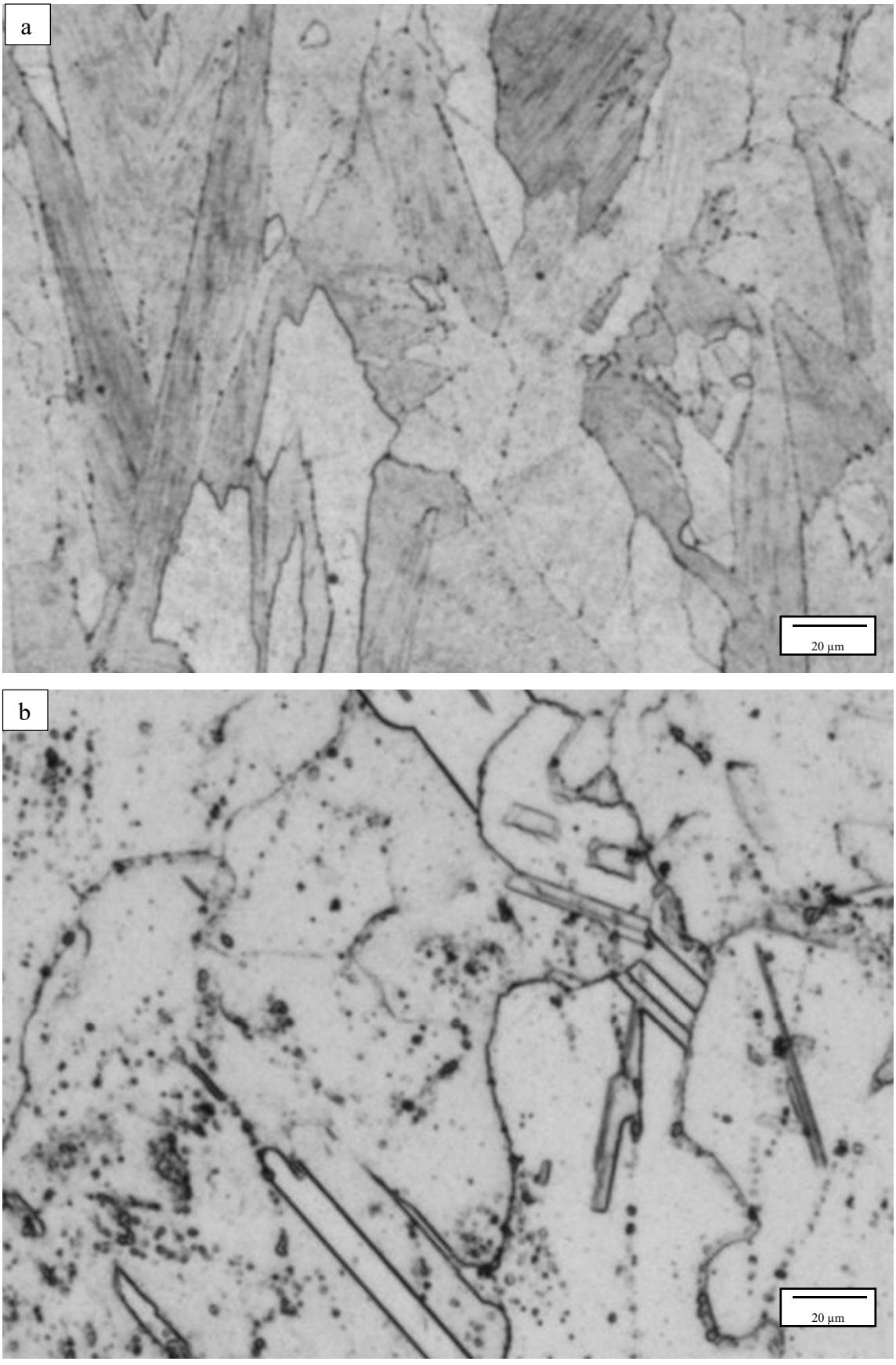

Figure 4. Magnified OM images of Variant 3 (**a**) and Variant 4.2 (**b**).

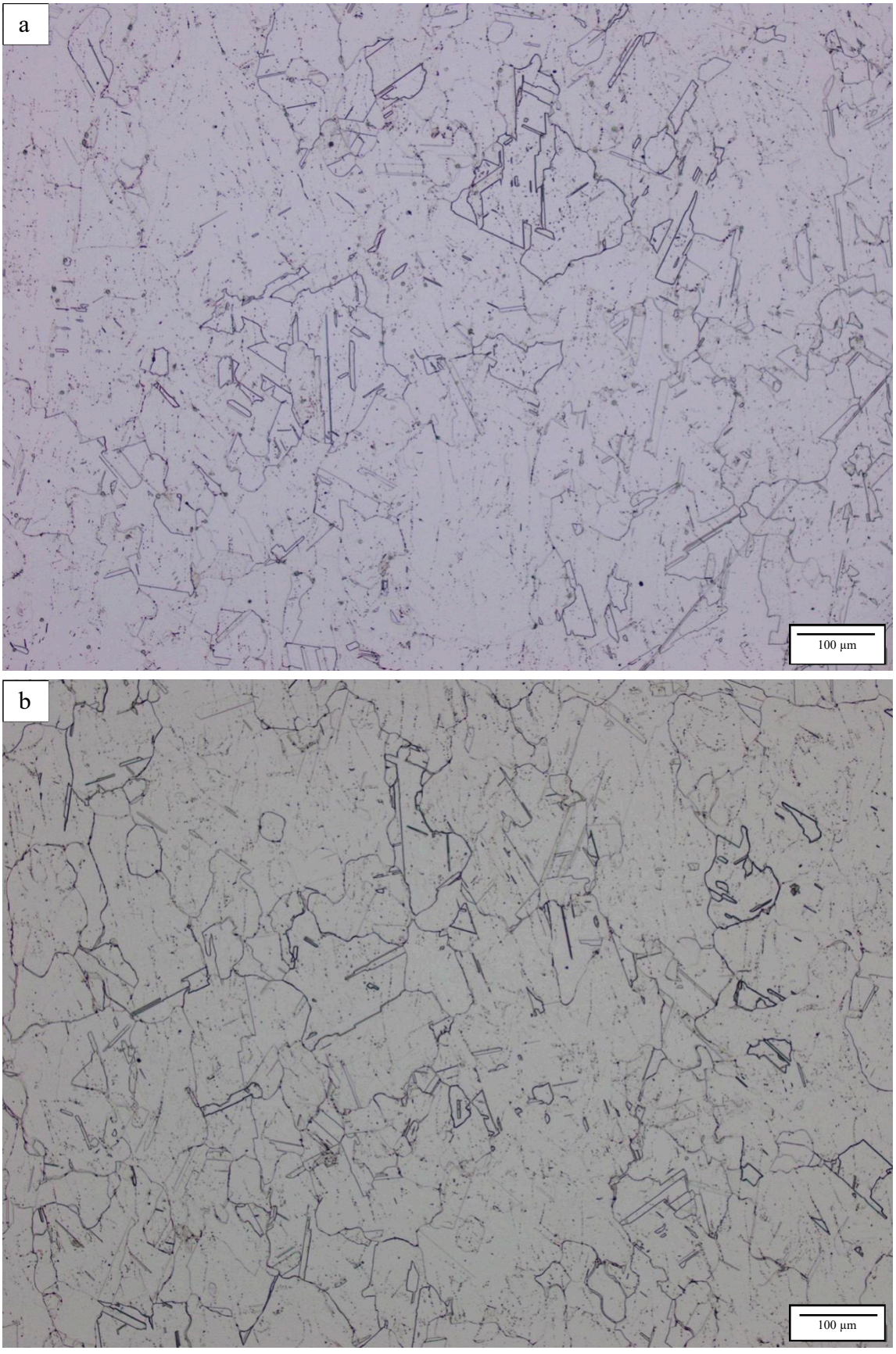

Figure 5. OM images for Variant 6 (**a**) and Variant 7 (**b**) (Table 1).

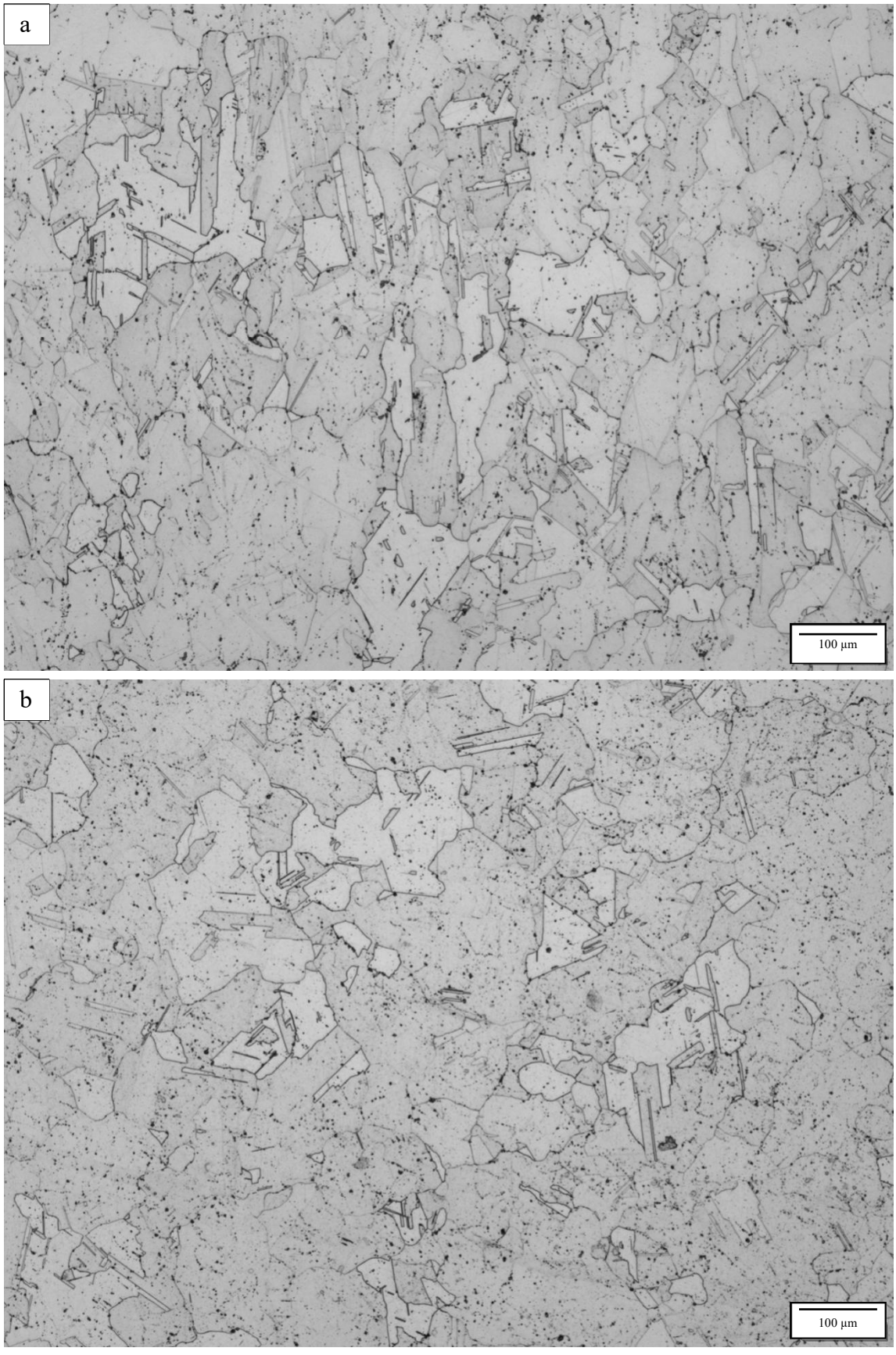

Figure 6. OM images for Variant 8 (**a**) and Variant 9.2 (**b**) (Table 1).

3.2. Mechanical Property Analysis and Comparisons

Table 2 lists the nominal (average) yield stress, UTS, and elongation for the experimental variant tensile measurements, along with corresponding density, hardness (HRC), and grain size measurements. It can be observed that, although there is only a small tensile yield stress difference between the as-built 718 alloy product (Variant 1) and the stress-relief annealed specimen (Variant 2), the elongation increases by ~64% while the hardness decreases correspondingly by 15%. These differences are reflected in the comparative microstructures shown in Figure 2. The other notable differences in mechanical properties shown in Table 2 occur on comparing Variant 2 with Variant 3, where the yield stress more than doubles, while the elongation is decreased by a factor of 3.3. The hardness also increases by 64%. This is due to the hardening-induced nano-precipitation resulting in the grain boundaries and grain interiors for Variant 3 as a consequence of solutionizing and aging, and these features are shown in Figures 3a and 4a. However, from Variant 4.1 to 9.2 in Table 2, the yield stress varies from 1.07 to 1.17 GPa (~9%), UTS from 1.32 GPa to 1.38 GPa (~6%), elongation from 11.4% to 19% (a change of ~67%), and a hardness change of ~8%. In the extreme, the hardness change from Variant 2 to Variant 4.2, for example, is ~61%, while the elongation between Variant 2 and Variant 8 decreased by a factor of 2.8. The equiaxed grain sizes were from Variants 4.2 to 9.2 (Figures 3b, 4b, 5b and 6b vary from 30 to 39 microns (~30%)). Table 2 also shows densities varying from ~8.11 to 8.20 g/cm^3. This variation is comparable to those measured in recent work by Kuo, et al. [7] (8.11 to 8.24 g/cm^3) for heat treatment of SLM-fabricated Inconel 718.

Table 2. Mechanical Properties and Related Data.

Inconel 718 Properties						
Variant	**Yield Stress**	**UTS**	**εmax**	**Density**	**Hardness**	**Grain Size**
	GPa	**GPa**	**Elong.**	**(g/cm^3)**	**(HRC)**	**μm**
1	0.64	0.98	26.3%	8.13	38	18
2	0.60	0.92	43.1%	8.11	33	22
3	1.26	1.40	12.6%	8.15	54	24
4.1	1.14	1.35	18.0%	8.12	52	38
4.2	1.13	1.35	17.2%	8.14	53	39
5	1.07	1.33	19.0%	8.14	49	33
6	1.15	1.36	14.3%	8.20	52	35
7	1.07	1.32	16.3%	8.18	49	32
8	1.16	1.36	11.4%	8.12	51	33
9.1	1.16	1.38	15.0%	8.15	52	30
9.2	1.17	1.38	11.6%	8.13	53	49

It is apparent in Table 2, and with reference to Table 1, that heat treatment schedule strategies can allow a wide range of choices for mechanical properties for SLM-fabricated Inconel 718 components. And while more conventional post-process heat treatments involving solutionizing and aging treatments produce a range of precipitation hardening, as shown for Variant 3 (Table 1) (Figure 4a) [6–12,18], heat treatments dominated by HIP temperatures in excess of 1120 °C uniformly result in recrystallized, equiaxed grains of only tens of microns containing annealing twins and carbides. Consequently, HIP treatments dominate the heat treatment strategies for manipulating microstructures and associated mechanical properties for Inconel 718 alloy. This is readily apparent in comparing the similar microstructures for Figures 3b, 4, 5 and 6 with the tensile properties shown in Table 2, where the yield stresses vary by only about 4% while the elongations vary by ~64% (11.6% to 19% for Variants 9.2 and 5, respectively).

4. Summary and Conclusions

This study has presented a wide range of post-SLM processing heat treatments of Inconel 718 alloy ranging from simple stress-relief anneal or simple HIP, to multiple treatment cycles including stress-relief

anneals, HIP, solutionizing and aging; including high temperature solutionizing, which dissolves most precipitate phases except for MC carbides, and produces recrystallized, equiaxed grains containing annealing twins. These various heat treatment cycles produced residual mechanical properties involving tensile yield strength and elongation variations from 1.26 GPa and 12.6% for stress-relief anneal and standard solutionizing and aging, to 1.07 GPa and 19% for stress-relief anneal and HIP at 1163 °C. These values can be compared with simple stress-relief anneal at 1065 °C, which produced a tensile yield stress of 0.60 GPa and elongation of 43%. Corresponding Rockwell C-scale hardness (HRC) values ranged from 33 for a yield stress of 0.60 GPa to 54 for a yield stress of 1.26 GPa. Microstructures for the as-fabricated Inconel 718 consisted of cellular microdendrites in small (18 micron) directional grains, which were recrystallized to equiaxed grains ranging from ~30 to 49 microns, and containing annealing twins and carbides at grain boundaries and intragrain regions for HIP treatment cycles above 1060 °C. Carbide precipitates were not observed to nucleate and grow on the coherent {111} twin boundaries as a consequence of their very low interfacial free energy relative to the regular grain boundaries. It can be concluded that for any HIP-inclusive heat treatment cycles where the HIP temperature is above 1060 °C, equiaxed, twinned grain structures containing carbides dominate Inconel 718 microstructures and associated mechanical behavior.

Author Contributions: Conceptualization, J.V., M.A., D.G., F.M.; Experiments and data, J.V., J.M., C.P., A.A.-I., E.A., M.A., D.G.; Research administration, E.A., F.M., Writing and editing, L.E.M., J.V., F.M., R.B.W. All authors have read and agreed to the published version of the manuscript.

Funding: This research received no external funding.

Acknowledgments: The research presented here was conducted at The University of Texas at El Paso within the W.M. Keck Center for 3D Innovation (Keck Center), a 13,000-sq. ft. state-of-the-art additive manufacturing facility. Additionally, equipment housed within the Department of Metallurgical, Materials and Biomedical Engineering was utilized. Support for the research was provided, in part, by MacIntosh Murchison Chair I in Engineering (RBW and SZU) with strategic investments in development of this work by the UTEP Mechanical Engineering Department and the W.M. Keck Center for 3D Innovation. The Authors are grateful to Miguel Lopez, and Bryan Ruvalcaba for their participation and contributions.

Conflicts of Interest: The authors declare no conflicts of interest.

References

1. Sims, C.T.; Hagel, W.C. *The Superalloys*; Wiley: New York, NY, USA, 1972.
2. Keiser, D.D.; Brown, H.C. *A Review of the Physical Metallurgy of Alloy 718*; Aerojet Nuclear Co.: Rancho Cordova, CA, USA, 1976; ANCR-1292. [CrossRef]
3. Reed, R.C. *The Superalloys: Fundamentals and Applications*; Cambridge Univ. Press: Cambridge, UK, 2006.
4. Ott, E.A.; Groh, J.R.; Banik, A.; Dempster, I.; Gabb, J.P.; Liu, X.; Mitchell, A.; Sjoberg, G.P.; Musatowska-Sarnok, A. (Eds.) *Superalloy 718 and Derivatives*; Wiley: New York, NY, USA, 2010.
5. Huan, G. Review of Inconel 718 alloy: Its history, properties, processing and developing substitutes. *J. Mater. Eng.* **2012**, 2, 92–100.
6. Nandwana, P.; Kirka, M.; Okello, A.; Dehoff, R. Electron beam melting of Inconel 718: Effects of processing and post-processing. *Mater. Sci. Technol.* **2018**, *34*, 612–619. [CrossRef]
7. Kuo, Y.-L.; Nagahari, T.; Kakehi, K. The effect of post-processes on the microstructure and creep properties of alloy 718 built up by selective laser melting. *Materials (Basel)* **2018**, *11*, 996. [CrossRef] [PubMed]
8. Seede, R.; Mostafa, A.; Brailovski, V.; Jahazi, M.; Medraj, M. Microstructural and microhardness evolution from homogenization and hot isostatic pressing on selective laser melted Inconel 718: Structure, texture, and phases. *J. Manuf. Mater. Process.* **2018**, 2, 30. [CrossRef]
9. Deng, D.; Peng, R.L.; Brodin, H.; Moverare, J. Microstructure and mechanical properties of Inconel 718 produced by selective laser melting: Sample orientation dependence and effects of post heat treatments. *Mater. Sci. Eng. A* **2018**, *713*, 294–306. [CrossRef]
10. Holland, S.; Wang, X.; Chen, J.; Cai, C.; Yan, F.; Li, L. Multiscale characterization of microstructures and mechanical properties of Inconel 718 fabricated by selective laser melting. *J. Alloy. Comp.* **2019**, *784*, 182–194. [CrossRef]

11. Balachandramurthi, A.R.; Moverare, J.; Mahade, S.; Pederson, R. Additive manufacturing of alloy 718 via electron beam melting: Effect of post-treatment on the microstructure and mechanical properties. *Materials (Basel)* **2019**, *12*, 68. [CrossRef] [PubMed]
12. Sindhura, D.; Sravya, M.V.; Murthy, G.V.S. Comprehensive microstructural evolution of precipitation in Inconel 718. *Met. Microstruct. Anal.* **2019**, *8*, 233–240. [CrossRef]
13. Wei, X.; Zheng, W.; Song, Z.; Lei, T.; Yang, Q.; Kie, C. Static recrystallization behavior of Inconel 718 alloy during thermal deformation. *J. Wuhan Univ. Technol.-Mater. Sci. Ed.* **2014**, *29*, 379–387. [CrossRef]
14. Cao, Y.; Bai, P.; Liu, F.; Hou, X.; Guo, Y. Effect of solution temperature on precipitates and grain evolution of IN 718 fabricated by laser additive manufacturing. *Materials (Basel)* **2020**, *13*, 340. [CrossRef] [PubMed]
15. Helmer, H.E.; Korner, C.; Singer, R.F. Additive manufacturing of nickel-based superalloy Inconel 718 by selective electron beam melting: Processing window and microstructureFocus Issue: The Materials Science of Additive Manufacturing. *J. Mater. Res.* **2014**, *29*, 1987–1996. [CrossRef]
16. Kershavarzkermani, A.; Sadowski, M.; Ladani, L. Direct metal laser melting if Inconel 718: Process impact on grain formation and orientation. *J. Alloy. Comp.* **2018**, *736*, 297–305. [CrossRef]
17. DebRoy, T.; Wei, H.L.; Zuback, J.S.; Mukerjee, T.; Milewski, J.O.; Beese, A.M.; Wilson-Heid, A.; De, A.; Zhang, W. Additive manufacturing of metallic components; Process, structure, properties. *Prog. Mater. Sci.* **2018**, *92*, 113–224. [CrossRef]
18. Radevich, J.F. The Physical Metallurgy of Cast and Wrought Alloy 718. In *Superalloy 718-Metallurgy and Applications*; The Minerals, Metals and Materials Society: Pittsburgh, PA, USA, 1989. [CrossRef]
19. Xu, S.; Dickson, J.I.; Koul, A.K. Grain growth and carbide precipitation in superalloy Udimet 520. *Met. Mater. Trans.* **1998**, *29*, 2687–2695. [CrossRef]
20. Hassan, B.; Corney, J. Grain boundary precipitation in Inconel 718 and ATI 718 plus. *Mater. Sci. Technol.* **2017**, *33*, 1879–1889. [CrossRef]
21. Trillo, A.E.; Murr, L.E. Effects of carbon content, deformation, and interfacial energetics on carbide precipitation and corrosion sensitization in 304 stainless steel. *Acta Mater.* **1999**, *42*, 235–245. [CrossRef]
22. Segura, I.A.; Murr, L.E.; Terrazas, C.A.; Bermudez, D.; Mireles, J.; Injeti, V.S.V.; Li, K.; Yu, B.; Misra, R.D.K.; Wicker, R.B. Grain boundary and microstructure engineering of Inconel 690 cladding on Stainless steel 316L using electron beam powder bed fusion additive manufacturing. *J. Mater. Sci. Technol.* **2019**, *35*, 351–367. [CrossRef]
23. Murr, L.E. *Interfacial Phenomena in Metals and Alloys*; Addison-Wesley Publishing Co.: Reading, MA, USA, 1975.
24. Da Cruz Gallo, F.; De Azevedo, L.M.B.; Labra, C.; Araujo, L.S.; Dille, J.; De Almeida, L.H. Correlation between grain boundary character distribution and delta-phase precipitation in nickel-based superalloy 718. *J. Mater. Res. Technol.* **2020**, *9*, 1801–1808. [CrossRef]